ACS Catalysis

pubs.acs.org/acscatalysis
Research Article

In Situ Development of a 3D Cu-CeO_2 Catalyst Selective in the Electrocatalytic Hydrogenation of Biomass Furanic Compounds

Giancosimo Sanghez de Luna, Patrick Zeller, Eylül Öztuna, Francesco Maluta, Andrea Canciani, Francesca Ospitali, Phuoc H. Ho, Alessandro Paglianti, Axel Knop-Gericke, Giuseppe Fornasari, Juan J. Velasco-Vélez,* and Patricia Benito*

Cite This: ACS Catal. 2023, 13, 12737−12745
Read Online

ACCESS | Metrics & More | Article Recommendations | Supporting Information

ABSTRACT: The renewable electricity-driven electrocatalytic hydrogenation of biomass-derived furanic compounds produces biopolymer (polyurethane) precursors under mild reaction conditions. The widely used Ag and Cu electrocatalysts failed in the selective conversion of the aldehyde into the alcohol in concentrated electrolytes due to the contribution of the electrodimerization. Herein, we proposed 3D CeO_2-based catalysts for the electrocatalytic hydrogenation of 5-hydroxymethylfurfural (HMF) electrolytes (0.02, 0.05, and 0.10 M) to 2,5-bishydroxymethylfuran (BHMF). An electrodeposition approach was adopted to coat CeO_2 on Cu open-cell foams. The ex-situ characterization of electrocatalysts revealed that they were made of a CeO_2 layer containing Cu species. The migration of Cu from the foam to the coating started during the electrodeposition, while the electroreduction conditions provoked the formation of Cu particles. The in situ characterization by X-ray absorption spectroscopy evidenced that the Ce^{4+} to Ce^{3+} reduction occurred just after the application of the cathodic potential; moreover, copper species were reduced to Cu^0 during the experiments. The combination of partially reduced CeO_2 and Cu particles not only provided selective reaction sites but also increased the electrical conductivity of the electrode. Consequently, the in situ-developed Cu-CeO_2 electrocatalysts promoted the selective electrocatalytic hydrogenation of the more concentrated 0.10 M HMF electrolytes, overperforming previously reported AgCu materials at −0.51 V vs RHE.

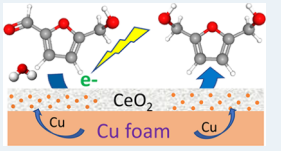

KEYWORDS: *copper, ceria, electrocatalyst, 5-hydroxymethylfurfural, in situ characterization, X-ray spectroscopy*

INTRODUCTION

CeO_2, a support widely used in thermo-catalytic processes,[1] is gaining increasing interest in electrocatalysis.[2−5] The Ce^{3+}/Ce^{4+} redox properties, oxygen vacancies, stability in basic media, and ability to disperse and stabilize both oxide and metallic particles were exploited in the hydrogen evolution reaction (HER) and oxygen reduction reaction (ORR) in alkaline media as well as in CO_2 and N_2 reduction (CO_2RR and N_2RR). Small metallic particles or even metal clusters dispersed on CeO_2 resulted in catalysts with a large electroactive surface area and in turn a high activity (e.g., Ni,[6−8] Ru,[9−11] Au,[12,13] and Cu[14]). However, CeO_2 was more than a simple support; the oxygen vacancies favored adsorption and activation of H_2O,[15] CO_2,[14] and N_2,[13,16,17] and recently also the C−N coupling in the synthesis of urea.[18] The metal−CeO_2 interface optimized the hydrogen binding and water absorption/dissociation energies[10] and enhanced CO_2 activation and could stabilize CO_2RR intermediates.[12,19] The synergistic effect of the metal−CeO_2 interface was also extended to cerium hydroxide; for instance, in combination with Cu, a $Ce(OH)_x$ film modified the water dissociation mechanism, and in turn the H_{ads} (adsorbed H) formation.[20]

It was therefore agreed that the electrocatalytic activity of CeO_2 depended on the Ce^{3+}/Ce^{4+} ratio and in turn on the oxygen vacancies. These properties were altered during electrochemical reduction due to either the cathodic potential[19,20] or the in situ generated H_2;[21] therefore, the identification of the active sites was tricky whenever only ex-situ characterization techniques were employed. It should be noted that the reduction of Ce^{4+} to Ce^{3+} also modified the CeO_2 electrical conductivity and the properties of the metals supported on it. For instance, in the Cu-CeO_x solid solution, the rapid electron transport channel provided by Ce^{3+} was reported to suppress the accumulation of electrons around Cu^{2+} sites, thereby protecting them from electrochemical reduction during CO_2 electroreduction to CH_4.[22]

Despite all the aforementioned CeO_2 advantages, to the best of our knowledge, it was not applied in the electrocatalytic reduction/hydrogenation of biomass-derived compounds such as benzaldehyde (a model component of bio-oil), furfural, or 5-hydroxymethylfurfural (HMF).[23,24] Only one work used CuO/CeO_2 on copper foam for the oxidation of HMF.[25] However, the potential of CeO_2 in this field could be huge. As an example, its ability to disperse metals, such as Ag, Cu, and Ni, and modify the water dissociation mechanism could foster selectivity in the

Received: July 22, 2023
Revised: August 24, 2023
Published: September 15, 2023

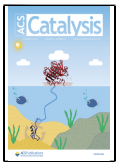

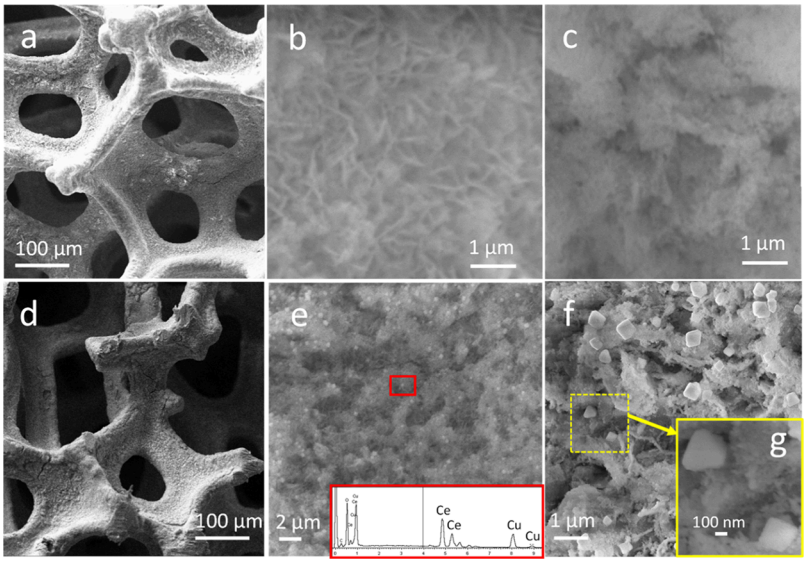

Figure 1. Characterization of CeO_2/Cu foam electrodeposited at −0.9 V vs SCE (−0.3605 V vs RHE) for 100 s with a 0.15 M $Ce(NO_3)_3$ electrolyte: (a−c) SEM images of the as-deposited catalyst; (d−g) SEM images of the spent catalyst. Energy-dispersive spectroscopy (EDS) spectrum recorded in the region of interest inside the red square. The spent catalyst was tested for ca. 25 h in the reaction conditions reported in Figure 3 and Figure S2 with all three 0.02, 0.05, and 0.10 M HMF electrolytes (including LSVs in borate and HMF).

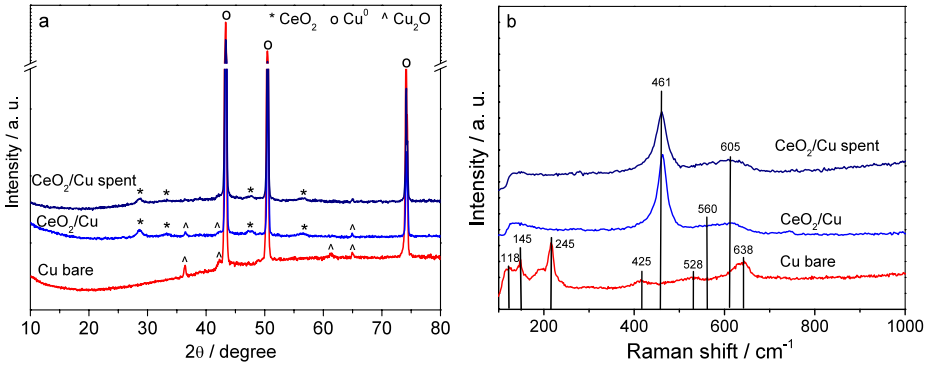

Figure 2. XRD patterns (a) and micro-Raman spectra (b) of CeO_2/Cu foam as deposited and after electrocatalytic tests. For comparison purposes, the characterization of Cu bare foam is included. Electrodeposition conditions: −0.9 V vs SCE (−0.3605 V vs RHE) for 100 s with a 0.15 M $Ce(NO_3)_3$ electrolyte. The spent catalyst was tested for ca. 25 h in the reaction conditions reported in Figure 3 and Figure S2 with all the three 0.02, 0.05, and 0.10 M HMF electrolytes (including LSVs in borate and HMF).

conversion of the aldehyde group of furanic or aromatic compounds to the alcohol in concentrated electrolytes. It could avoid the radical coupling side reaction (electrodimerization), which is currently the main bottleneck of the electrocatalytic process for a further deployment.[24]

Herein, we propose for the first time in situ activated Cu-CeO_2/Cu open-cell foams for the electrocatalytic conversion of biomass-derived furanic compounds. We focused on the conversion of HMF, obtained from waste lignocellulosic biomass, to 2,5-bishydroxymethylfuran (BHMF), a chemical for polymer production (e.g., polyurethane), at pH = 9.2.[26] The catalysts were prepared by a simple one-step electrodeposition of CeO_2 on the surface of Cu open-cell foams, modifying the thickness of the coating deposited. The chemical, physical, electrochemical, and electrical properties of the materials were investigated, and their activities were assessed in the electrocatalytic conversion of 0.02 to 0.10 M HMF solutions into BHMF. The catalysts were also characterized in situ by X-ray absorption near-edge structure spectroscopy (XANES) to identify the changes of the catalyst under the reaction conditions and the real active species involved in the electrocatalytic process. These aspects were the clue to evaluating the aforementioned CeO_2 reduction but also the changes in copper species. We demonstrated that the in situ development of Cu particles, well dispersed and stabilized, on the CeO_2 support not only provided selective sites for the reaction but also increased the electrical conductivity of the CeO_2. This electrocatalyst reached a 99% conversion of 0.10 M HMF solutions with a 75% selectivity in BHMF (74% FE, Faradaic efficiency) and evidenced that Ag can be avoided in the catalyst. To the best of our knowledge, it overperforms the most active Ag and AgCu catalysts[27−31] and achieves performance equivalent to that of noble metals[32] reported in the literature.

RESULTS AND DISCUSSION

As-Deposited Catalyst Characterization. A compact coating of ca. 0.5−1 μm was evenly distributed on the surface of the Cu open-cell foam after electrodeposition at −0.9 V versus SCE (−0.3605 V versus RHE) for 100 s with an 0.15 M $Ce(NO_3)_3$ electrolyte, as can be seen by scanning electron microscopy (SEM) (Figure 1a). The coating was made by arrays

https://doi.org/10.1021/acscatal.3c03363
ACS Catal. 2023, 13, 12737−12745

of platelet-like particles with a well-defined growth direction (Figure 1b) and spherical particles (Figure 1c). X-ray diffraction (XRD) proved the formation of the cubic CeO_2 phase during electrodeposition (Figure 2a) with crystallite sizes around 7.5 nm (Table S1). Notably, Cu_2O was present due to Cu foam oxidation either by contact with air or during the synthesis. Micro-Raman spectroscopy indicated the presence of defects in the CeO_2 structure (Figure 2b). Together with the F_{2g} band at 461 cm^{-1}, the bands at 560 and 605 cm^{-1} developed, which could be related to oxygen vacancies developed due to the inclusion of cations within the CeO_2 structure and the formation of Ce^{3+}, respectively.[22,33,34] It should be noted that in the spectra of coated samples, the bands of Cu_2O are not detected; only in few regions of interest, where the CeO_2 layer is thin and there are some cracks, are Cu_2O bands registered. The characterization of the samples by XANES evidenced that cerium was electrodeposited as Ce^{4+} (Figure S1), hence suggesting that the contribution of Ce^{3+} in the as-prepared catalyst was marginal. The direct deposition of the CeO_2 phase rather than the hydroxide previously reported in the literature[20] could be related to differences in the pH reached during the electrodeposition.

Electrocatalytic Conversion of HMF. The CeO_2/Cu electrocatalyst was tested in the reduction of HMF electrolytes at increasing concentrations (0.02, 0.05, and 0.10 M) by applying a constant potential of −0.51 V vs RHE (Figure 3),

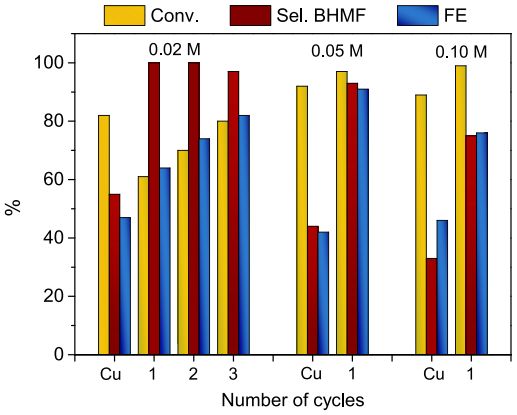

Figure 3. Electrocatalytic performance of CeO_2/Cu foam in the reduction of HMF to BHMF at −0.51 V vs RHE modifying the HMF concentration in the electrolyte (0.02, 0.05, and 0.10 M HMF). All of the tests were performed over the same CeO_2/Cu foam. For comparison purposes, the data obtained for Cu bare foam are included. Electrodeposition: −0.9 V vs SCE (−0.3605 V vs RHE) for 100 s with a 0.15 M $Ce(NO_3)_3$ electrolyte.

selected in our previous work.[35] The pH was 9.2 to favor the production of BHMF in agreement with former results.[26,36] The electrocatalyst selectively converted the dilute 0.02 M HMF electrolyte into BHMF (selectivity close to 100%), largely outperforming a Cu bare foam that only reached 55% selectivity. Remarkably, a steady improvement in the HMF conversion was observed by repeating the electroreduction of 0.02 M HMF solutions for three cycles, achieving a conversion of 80% in the last cycle. The high selectivity toward BHMF of the CeO_2/Cu foam catalyst was also demonstrated in the reduction of 0.05 and 0.10 M HMF electrolytes. The BHMF selectivity was around 90% for the 0.05 M and 75% for the 0.10 M, overperforming the results obtained by our previously reported AgCu catalyst[31,35] and others reported in the literature.[27−30] The BHMF productivity increased with the HMF concentration, 0.203 and 0.414 mmol/cm^2 h in 0.05 and 0.10 M HMF electrolytes, respectively. The repetition of the electrolysis with the 0.02 M HMF electrolyte after the tests with the more concentrated solutions did not show any important deactivation phenomena; contrarily, the conversion further increased. Meanwhile, the selectivity slightly decreased, keeping the FE constant (Figure S2). The total reaction time of the catalyst was ca. 25 h. The reproducibility of the performance was assessed by repeating the tests over different CeO_2/Cu catalysts with 0.05 and 0.10 M HMF electrolytes, and average BHMF selectivities were 85 and 74%, respectively (Figure S3a,b). The stability of the catalyst was also confirmed by performing three cycles with the 0.05 M HMF electrolyte, which showed similar results (Figure S3c). It is noteworthy that the coating of Ag by electrodeposition on the CeO_2/Cu foam did not provide any remarkable improvement in the activity (Figure S4 and Table S2).

Electrochemical and Chemical−Physical Characterization. To explain the performance of the CeO_2/Cu catalysts and the activation observed with the reaction time, their electrochemical properties were investigated and the spent catalysts were characterized. Linear sweep voltammograms (LSVs) in HMF-free and -containing electrolytes were recorded and compared with those obtained for the bare Cu foam (Figure 4). In the HMF-free electrolyte, an enhancement in the HER activity due to the presence of CeO_2 was measured, visible by the shift of the onset toward less cathodic potential in comparison to the bare Cu foam and the increase in the current density exchanged (Figure 4a). Tafel slopes in borate and 0.05 M HMF electrolytes (Figure S5) confirmed that the HMF reduction occurred faster (70 mV/dec) than the HER (114 mV/dec), in agreement with previous results.[31] However, it should be noted that the kinetics at potentials close to the onset were very slow, likely due to the contribution of the reduction of Ce^{4+} to Ce^{3+} and Cu^{2+} to Cu^0;[21] hence, the values here reported were obtained at more cathodic potentials (see Figure S5). A careful examination of the shape of the LSVs revealed that the activity in the HER was likely modified during the electrocatalytic cycles with the 0.02 M HMF electrolyte (Figure S6). The current exchanged above −0.5 V vs RHE decreased in both the absence and presence of HMF. The smaller contribution of the HER could explain the increase in the HMF conversion and the FE, as well as the longer time to accumulate the charge. After this initial modification, the shape of the LSVs was rather stable. An in-depth investigation of the kinetics and reaction mechanism is required to further support the hypotheses. The capacitance (C_{DL}) values, measured after the first LSV in borate, were one order of magnitude higher for the CeO_2/Cu than for the Cu foam (Figure S7), suggesting a larger electroactive area in the former. The capacitance slightly increased after the third reaction cycle; however, it decreased when the measurement was preceded of a washing step, likely due to some changes in the catalyst (e.g., oxidation, vide infra).

In the diffraction pattern of the spent catalyst (Figure 2a), the reflections of Cu_2O were strongly reduced while the CeO_2 crystallite size was rather constant (7.4 to 7.7 nm, Table S1). However, the absence of the band at ca. 560 cm^{-1} in the Raman spectra (Figure 2b) suggested that CeO_2 defects were removed, mostly those related to the inclusion of Cu^{2+} into the oxide structure. SEM images confirmed the stability of the coating during tests (Figure 1d); only at a few points of the foam was some solid detachment observed after more than 25 h of electrocatalytic reduction (Figure S8). Nevertheless, high-magnification images revealed that the morphology and

https://doi.org/10.1021/acscatal.3c03363
ACS Catal. 2023, 13, 12737−12745

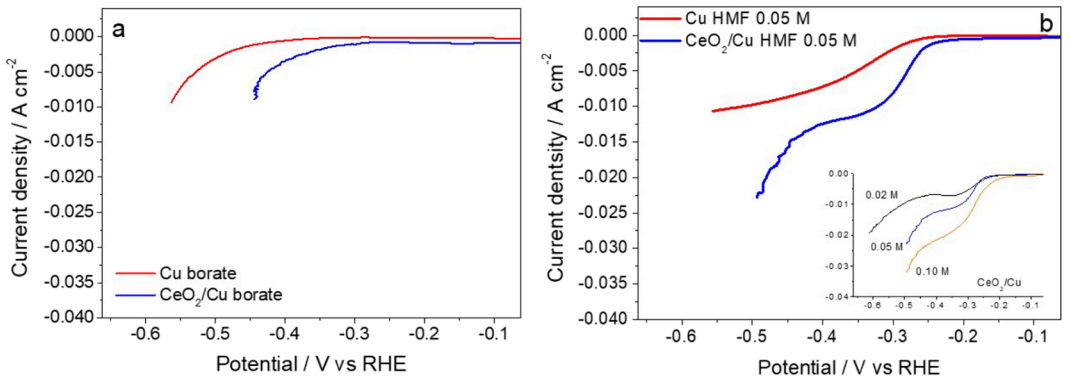

Figure 4. LSVs in borate buffer (a) and 0.05 M HMF + borate buffer (b) for the bare Cu foam and CeO_2/Cu foam. The inset in (b) is the plot of the LSV over the CeO_2/Cu foam with HMF electrolytes of different concentrations (0.02, 0.05, and 0.10 M HMF). Electrodeposition: −0.9 V vs SCE (−0.3605 V vs RHE) for 100 s with a 0.15 M $Ce(NO_3)_3$ electrolyte.

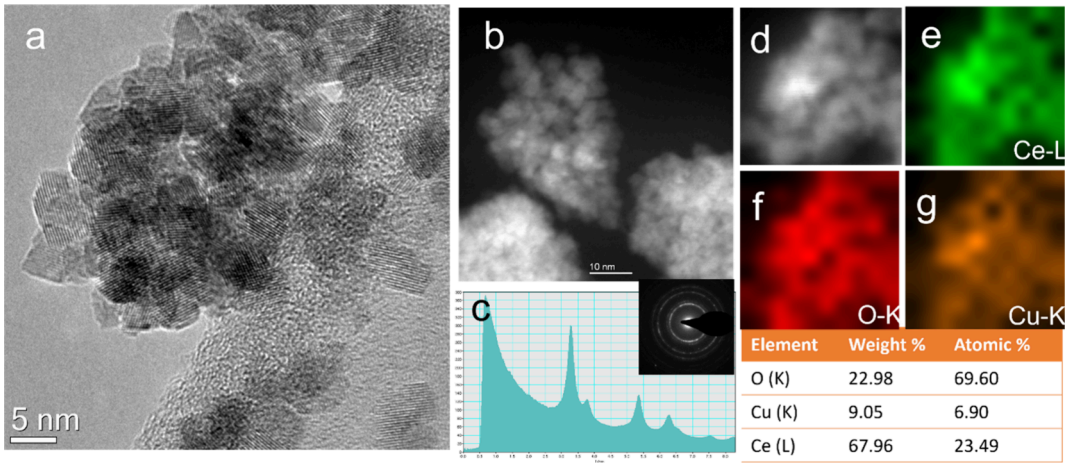

Element	Weight %	Atomic %
O (K)	22.98	69.60
Cu (K)	9.05	6.90
Ce (L)	67.96	23.49

Figure 5. HRTEM characterization of the as-deposited catalyst prepared at −0.9 V vs SCE (−0.3605 V vs RHE) for 100 s with the 0.15 M $Ce(NO_3)_3$ electrolyte. (a) HRTEM image; (b) HAADF STEM images of aggregates of nanoparticles; (c) SAED recorded in the whole area of b; (d−g) STEM/EDS analysis showing elemental maps of Ce, O, and Cu.

composition of the coated layer were substantially modified (Figure 1e−g, Figure S9). Round and truncated octahedron particles developed after electrocatalytic tests. Their morphology is characteristic for copper oxides (CuO, Cu_2O).[37] That the particles are Cu is also confirmed by EDS (Figure S9) and high-resolution transmission electron microscopy, HRTEM (Figure S10), analysis. Most likely, the particles formed as metallic Cu^0 and were oxidized after the reaction due to air contact. These results agreed with the recently reported electrochemical reconstruction of the surface of the copper foam−CuO/CeO_2 under reductive potential.[25] Despite the reconstruction of the catalyst and the formation of new copper particles on the catalyst surface, inductively coupled plasma atomic emission spectroscopy (ICP-AES) analyses discarded the leaching of both Cu and Ce.

In summary, it could be stated that copper from the support migrates to the coating of CeO_2 forming copper particles that enhanced the electrocatalytic performance of the catalyst. The formation of Cu particles on the surface of the foam, and therefore the activity improvement, is not observed by treating a Cu foam in a 0.1 M KNO_3 electrolyte under the same conditions as for depositing CeO_2 (−1.1. V vs SCE, −0.5605 V vs RHE, for 200 s) (Figure S11). Thus, reconstruction of the electrocatalyst surface occurs in the presence of CeO_2.

Role of the CeO_2 Layer Thickness. To further investigate the activity of the CeO_2/Cu catalysts, a 2.5−5 μm-thick layer (deposited mass ca. 105 mg, Table S1) but with the same structural features (i.e., CeO_2 nanocrystallites with defects) was prepared by modifying the electrodeposition conditions, i.e., 0.10 M $Ce(NO_3)_3$, −1.1 V vs SCE (−0.5605 V vs RHE), and 200 s (Figure S12).[38] This thicker layer could provide more catalytically active sites whenever the solid adhesion to the foam and the electrical conductivity were ensured; the insulator properties of CeO_2 could indeed hamper the application of these novel catalysts. The LSV curves recorded in both HMF-free and HMF-containing electrolytes did not evidence a substantial modification of the activity in the HER regardless of the coating thickness (Figure S13). The electrocatalytic reduction tests with the 0.05 and 0.10 M HMF electrolytes confirmed that CeO_2-containing Cu-based particles catalyze the electrochemical process (Figures S13 and S14).

Ex Situ and In Situ Characterization of the Catalysts during Their Lifetime. To better investigate the migration of copper onto CeO_2, the coatings were more deeply characterized at different steps of the catalyst lifetime, i.e., as prepared, after the first LSV in borate, and after several cycles of electrocatalytic HMF reduction.

The electrodeposition of nanometric CeO_2 was confirmed by HRTEM; the solid was made of thin platelets with sizes around

https://doi.org/10.1021/acscatal.3c03363
ACS Catal. 2023, 13, 12737−12745

2−8 nm, which aggregated, forming fragments of 20−80 nm (Figure 5a,b). These aggregates were also observed in SEM images (Figure 1); the plate-like morphology was not related to single particles but to the aggregated nanosized particles observed by HRTEM. Note that the size of the CeO_2 particles was not modified during electrocatalytic tests (Figure S10), in agreement with the crystallite size values obtained from XRD. STEM/EDS (scanning transmission electron microscopy/energy-dispersive spectroscopy) analyses of the as-prepared coating evidenced the presence of copper in the deposited solid (Figure 5d−g). However, neither selected area electron diffraction (SAED) patterns (Figure 5c) nor high-angle annular dark field (HAADF) images (Figure 5b) detected any copper-containing crystalline phase or particles, respectively. These results suggested the incorporation of Cu^{2+} into the CeO_2 structure, which could be responsible for the vacancies estimated by Raman. Note that Luo et al. have reported the formation of a Cu-modified $Ce(OH)_x$ by depositing the cerium film above a Cu foam.[20]

The characterization of the coating by SEM at three stages of its lifetime (after LSV in borate, electrocatalytic reduction for different numbers of reaction cycles) revealed some insights in the catalyst reconstruction. After the first LSV in borate, copper particles were observed within the catalytic coating (Figure S15a). Subsequently to HMF electrocatalytic reduction tests, a larger amount of poorly defined Cu particles developed (Figure S15b). The Cu particles grew and led to well-defined shapes when the number of reaction cycles increased (Figure 1, Figure S15c). The aforementioned increase in the capacitance was in agreement with the improvement in the activity and the observed increase in the Cu particles on the surface. Hence, it could be hypothesized that the Cu species located inside the CeO_2 matrix reduced and/or sintered under a cathodic potential, forming metallic or oxidic copper particles. Weng et al. have introduced a similar approach to generate metallic nanoparticles after the thermal reduction of $NiCeO_2$ solid solution.[39]

The electrochemical characterization and activity tests proved the feasibility of coating Cu foams with CeO_2 to selectively convert HMF into BHMF; however, the establishment of a structure−activity relationship is tricky. The enhanced electrocatalyst activity could be related to (i) dispersed copper particles; (ii) involvement of CeO_2 in the HMF reduction and/or HER; (iii) a synergistic effect between Cu and CeO_2; and (iv) an improvement in the electrical conductivity of the CeO_2 coating due to Cu particles. Finally, the oxidation state of both copper and cerium species could be modified with time on stream, and therefore all the above-commented features.

To investigate the role of copper nanostructuration, the results herein obtained with the CeO_2/Cu sample in the 0.05 M HMF electrolyte were compared with those obtained in our previous work over Cu nanoparticles deposited on a Cu foam;[31] see Table 1. Lower selectivity and FE were achieved by the Cu nanoparticles alone in comparison to those of the CeO_2/Cu catalyst. The beneficial effect of CeO_2 in the electrocatalytic HMF conversion to BHMF was also proven when the oxide coating was deposited on a Ag foam (Table 1). However, the productivity dropped to 0.05 mmol of BHMF/h cm^2, which could be related to the coating morphology (Figure S16).

The relative conductivity of the electrocatalysts was measured through electrical resistance tomography, ERT (Figure 6). By definition, the bare Cu foam had a mean dimensionless conductivity equal to unity. The coating of CeO_2 provoked a decrease in this value, in agreement with its insulator-like behavior. The conductivity of the CeO_2/Cu sample increased after LSV in borate and the electrocatalytic reduction of a 0.05 M HMF solution. The presence of segregated Cu particles could be responsible for the increased conductivity.[14] The foam substrate and the in situ grown Cu nanoparticles could behave as a conductive network, a role previously reported by carbonaceous material dispersed in the CeO_2.[40,41] The enhanced electrical conductivity could facilitate the reduction of CeO_2, but simultaneously a reduced CeO_2 could also favor the conductivity.[22]

The changes in the electronic structure of the catalysts were investigated in situ by XANES in total fluorescence yield mode (TFY) using the electrochemical cell described in the methods section at −0.61 V vs RHE. CeO_2 was electrodeposited on a silicon nitride membrane coated by physical vapor-deposited (PVD) Cu. For comparison purposes, Cu was also electrodeposited on PVD Cu. Due to experimental limitations, the PVD copper was used instead of a copper foam. Thus, the structural effects, derived from the different morphologies, were not taken into account in this study. However, no significant changes are expected in the electronic structure ascribed to the use of PVD or copper foams. On the other hand, the amount of coating deposited is lowered in comparison to the foam and therefore the number of reducible species. The measurements were performed in borate buffer (control experiment) and in borate + 0.05 M HMF. Figure 7 shows the *in situ* experiments for the different electrodes electrodeposited on PVD copper in 0.5 M borate, used as control experiments. The copper of the pure electrodeposited copper electrode was at the open-circuit voltage (OCV) mainly metallic with some contribution of

Table 1. Comparison of the Electrocatalytic Activity of CeO_2/Cu and Cu/Cu, and CeO_2/Ag and Ag[a]

catalyst	conv. (%)	sel. BHMF (%)	FE (%)
CeO_2/Cu	91	85	76
Cu/Cu[b]	92	72	66
CeO_2/Ag	87	79	80
Ag[b]	94	65	66

[a]Reaction conditions: 0.05 M HMF solutions in borate buffer at −0.51 V vs RHE. [b]from ref 31.

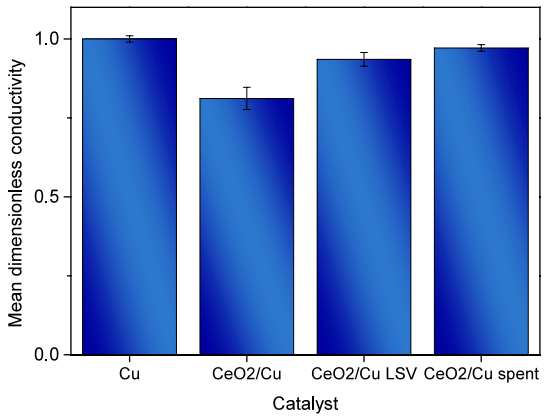

Figure 6. Mean dimensionless conductivity of the bare foam and of the electrocatalysts prepared with the 0.15 M $Ce(NO_3)_3$ electrolyte at −0.9 V vs SCE (−0.3605 V vs RHE) for 100 s along the three different steps of their lifetime. CeO_2/Cu: as prepared; CeO_2/Cu LSV: after the LSV in borate buffer; CeO_2/Cu spent: after the electroreduction of a 0.05 M HMF solution.

https://doi.org/10.1021/acscatal.3c03363
ACS Catal. 2023, 13, 12737−12745

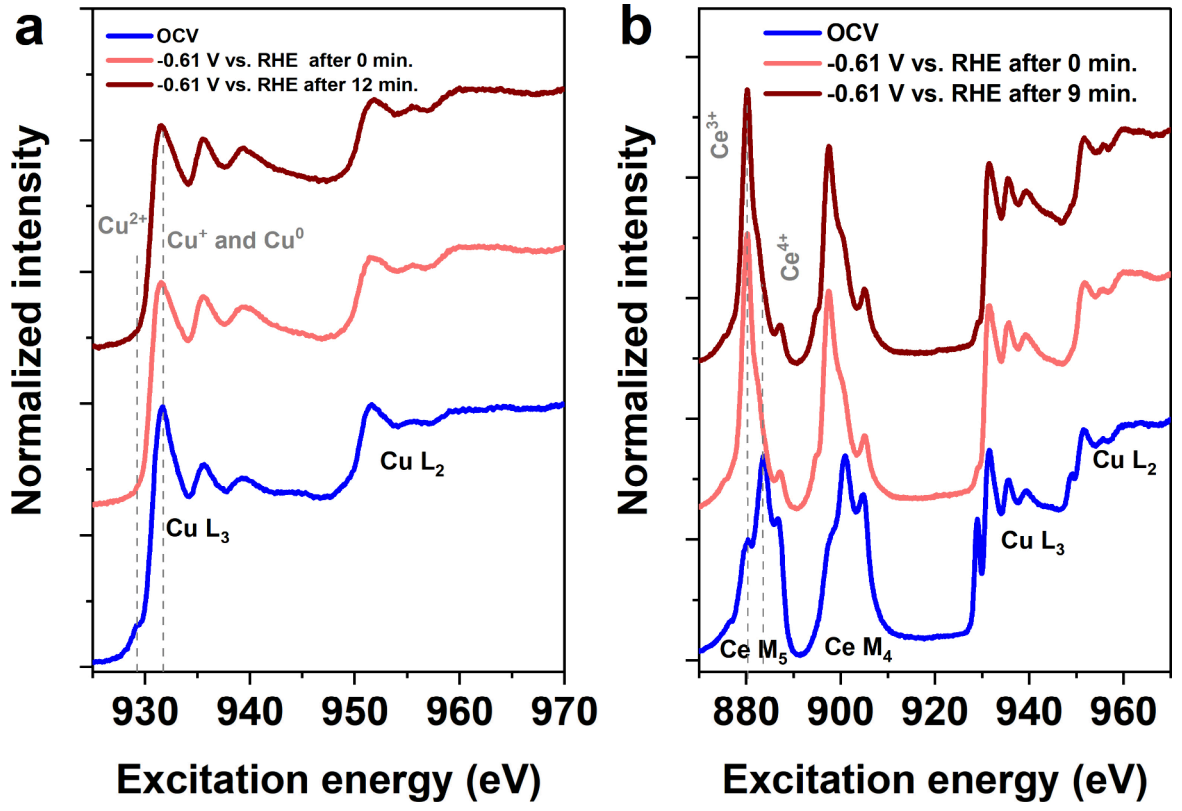

Figure 7. In situ XANES-TFY measurements collected in 0.5 M borate buffer at OCV and at −0.61 V vs RHE. (a) The spectra for a pure Cu sample. (b) The results from the CeO_2/Cu system. The sequence of measurements and electrochemical conditions is given in the legend: (a) 1. OCV, 2. −0.61 V vs RHE after 0 min, 3. −0.61 vs RHE after 12 min; (b) 1. OCV, 2. −0.61 V vs RHE after 0 min, 3. −0.61 vs RHE after 9 min. Positions of the main spectral features for each oxidation state are indicated by vertical, dotted lines. The samples were prepared in situ, as given in the SI.

Cu^{2+}/Cu^{+}, according to the peak shape.[42] Note that the majority of the signal came from the bulk of PVD Cu. The changes in the peak shapes reveal reduction of the Cu^{2+}/Cu^{+} contribution to Cu^0 at −0.61 V vs RHE (Figure 7a). More interesting results were found for the electrodeposited Ce electrodes at which the cerium was mainly in the form of CeO_2 at OCV, according to the reference peak shapes.[43] Applying a cathodic potential of −0.61 V vs RHE resulted in an immediate change of the signal shape (Figure 7b). This can be explained as a partial reduction from Ce^{4+} to Ce^{3+}, with Ce^{3+} being the majority phase. At the cathodic potential, the PVD copper electrode also reduced, but in contrast to the pure copper sample, a small fraction of the Cu^{2+} oxidation state remained.

In the second set of experiments, the same electrodeposited electrodes were investigated in the presence of a 0.5 M borate buffer + 0.05 M HMF electrolyte. In this case, the copper electrode also underwent its reduction at −0.61 V vs RHE to Cu^0, as shown in Figure 8a. For the case of the electrodeposited CeO_2 on PVD copper, Ce behaved similarly to the case without HMF and underwent its partial reduction from Ce^{4+} to Ce^{3+}; see Figure 8b. However, a main difference in comparison to the control experiments with borate buffer electrolyte was that Cu^{2+} species were not detected after several minutes of reaction time.

Taking into account all these set of experiments, we could conclude that, during the electrocatalytic hydrogenation of HMF to BHMF, Ce^{3+} species play a role in electroactivity. CeO_2 was mainly (>50%) reduced just after the application of the cathodic potential and then it remained mainly stable at that potential, though it oxidized back to Ce^{4+} once the cathodic potential was removed. Thus, the catalyst oxidized between the tests with borate and borate + HMF electrolytes. The high amount of reduction in CeO_2 at the cathodic potential applied during the in situ experiments indicates that Ce_2O_3 or $Ce(OH)_3$ is the important phase and not oxygen vacancies on CeO_2. The fact that the relevant phase can only be observed under reaction conditions underlines the importance of an in situ characterization of this material. For the copper, the reduction of Cu^{2+} to Cu^0 was not completed at −0.61 V vs RHE in the borate electrolyte but occurred under the presence of HMF. However, Raman spectra indicated the decrease of the vacancies generated by the inclusion of Cu^{2+} into the CeO_2 structure.

CONCLUSIONS

The selective electrocatalytic conversion of HMF electrolytes up to 0.10 M into BHMF was feasible over in situ developed 3D Cu-CeO_2-based catalysts. Meanwhile, the in situ characterization was mandatory to observe the catalyst under reaction conditions. An evenly nano-CeO_2 coating directly precipitated on the surface of Cu open-cell foams during the electrobase generation method. During the preparation, some Cu species were incorporated into the oxide coating. The application of a −0.51 V vs RHE potential both in borate buffer and in the reaction media (borate + HMF) provoked the reconstruction and reduction of the catalyst. At the cathodic potential (−0.61 V vs RHE), CeO_2 underwent a partial reduction from Ce^{4+} to Ce^{3+}, and Cu^{2+}/Cu^{+} was reduced to Cu^0. The quick oxidation of Ce^{3+} to Ce^{4+} at the OCV and in air made mandatory the in situ characterization of the catalysts to identify Ce^{3+} species. Moreover, we highlight the importance of developing techniques to better identify and quantify the number of active

https://doi.org/10.1021/acscatal.3c03363
ACS Catal. 2023, 13, 12737−12745

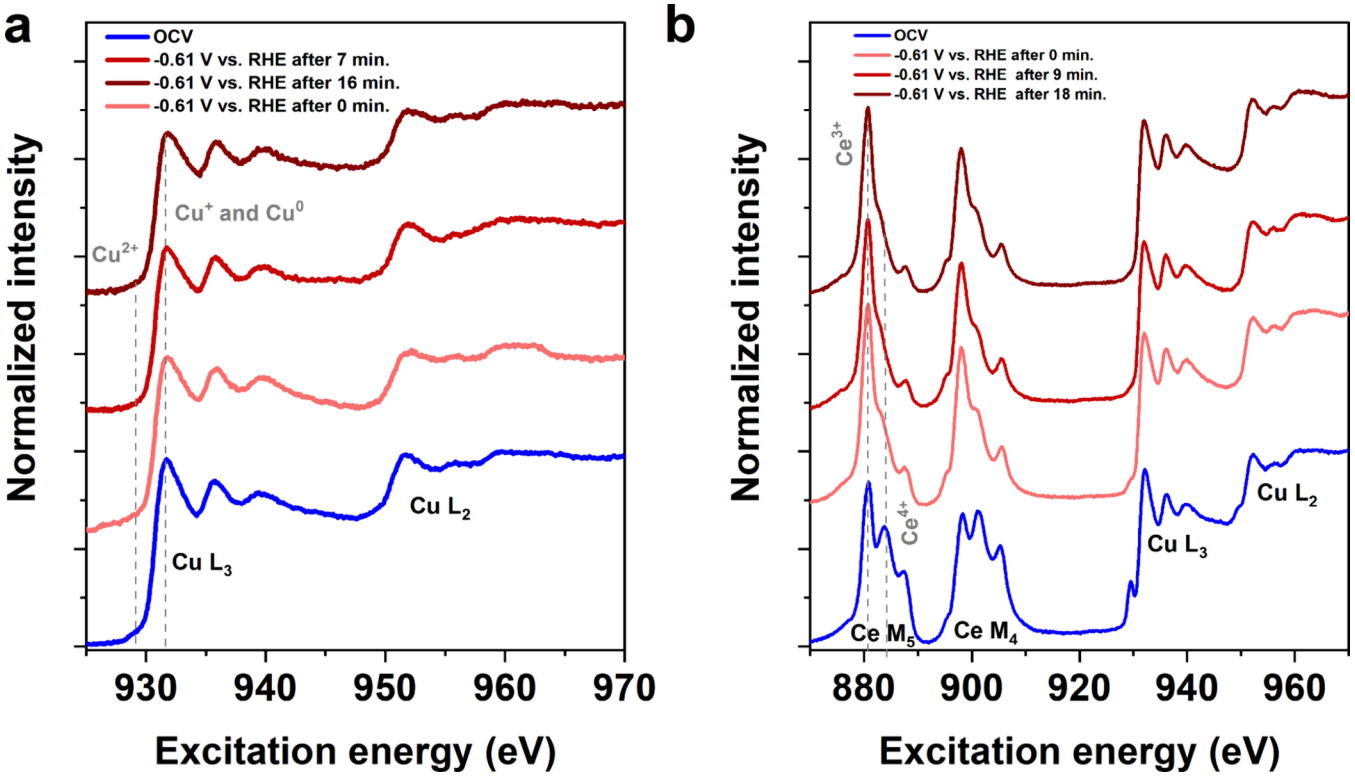

Figure 8. In situ XANES-TFY measurements collected in 0.5 M borate buffer + 0.05 M HMF at the OCV and at −0.61 V vs RHE. (a) The spectra for a pure Cu sample. (b) The results from the CeO_2/Cu system. The sequence of measurements and electrochemical conditions is given in the legend: (a) 1. OCV, 2. −0.61 V vs RHE after 0 min, 3. −0.61 vs RHE after 7 min, 4. −0.61 V vs RHE after 16 min; (b) 1. OCV, 2. −0.61 V vs RHE after 0 min, 3. −0.61 vs RHE after 9 min, −0.61 V vs RHE after 18 min. Positions of the main spectral features for each oxidation state are indicated by vertical, dotted lines. The samples were prepared in situ as given in the SI.

sites involved in the electrochemical conversion of biomass-derived aqueous electrolytes in complex electrocatalytic systems like the one here reported, containing unstable metallic species (susceptible to oxidation) and a reducible support.

The combination of Cu particles and partially reduced CeO_2 coatings fostered the selectivity of the process, providing active sites and enhanced electrical conductivity. This novel type of catalysts outperformed Ag-containing materials and could reach performances closer to noble-metal-based electrocatalysts during the selective conversion of 0.01 M HMF electrolytes. Hence, they could open the way for the further intensification of the electrocatalytic hydrogenation of biomass-derived furanic compounds.

■ ASSOCIATED CONTENT

Supporting Information

The Supporting Information is available free of charge at https://pubs.acs.org/doi/10.1021/acscatal.3c03363.

Experimental details, materials, and methods; XANES-TFY spectra of in situ electrodeposition of Cu and CeO_2/Cu onto PVD Cu electrodes; summary of the average of deposited mass after electrodeposition conditions and crystallite size of CeO_2 for as-deposited and spent catalysts; electrocatalytic performance of CeO_2/Cu foam in the reduction of 0.02 M HMF to BHMF; reproducibility and stability of the electrocatalytic performance of CeO_2/Cu catalysts; SEM images of the electrocatalytic activity of Ag/CeO_2/Cu; Tafel plots of the CeO_2/Cu catalyst in borate and 0.05 M HMF electrolytes; evolution of the LSVs in borate and HMF with the electrocatalytic reaction cycles for the CeO_2/Cu foam; scan-rate-dependent CV studies of the CeO_2/Cu catalyst to obtain C_{DL} values; SEM/EDS and HRTEM/STEM/HAADF/EDS characterization of spent catalysts; electrocatalytic activity of a Cu foam treated in KNO_3; SEM/XRD/Raman characterization and electrocatalytic activity of thick CeO_2/Cu coatings; SEM images of a spent coating after the first LSV in borate; SEM of a Ag foam coated by CeO_2 (PDF)

■ AUTHOR INFORMATION

Corresponding Authors

Juan J. Velasco-Vélez − *Fritz-Haber-Institut der Max-Planck-Gesellschaft, Berlin 14195, Germany; Max Planck Institute for Chemical Energy Conversion, Mülheim 45470, Germany; ALBA Synchrotron Light Source, Cerdanyola del Valles, Barcelona 08290, Spain*; Email: jvelasco@cells.es

Patricia Benito − *Department of Industrial Chemistry "Toso Montanari" and Center for Chemical Catalysis − C3, Alma Mater Studiorum, Università di Bologna, Bologna 40136, Italy*; Email: patricia.benito3@unibo.it

Authors

Giancosimo Sanghez de Luna − *Department of Industrial Chemistry "Toso Montanari", Università di Bologna, Bologna 40136, Italy*

Patrick Zeller − *Fritz-Haber-Institut der Max-Planck-Gesellschaft, Berlin 14195, Germany; Helmholtz-Zentrum Berlin für Materialien und Energie GmbH, BESSY II, Berlin 12489, Germany*

https://doi.org/10.1021/acscatal.3c03363
ACS Catal. 2023, 13, 12737−12745

Eylül Öztuna − *Fritz-Haber-Institut der Max-Planck-Gesellschaft, Berlin 14195, Germany; Helmholtz-Zentrum Berlin für Materialien und Energie GmbH, BESSY II, Berlin 12489, Germany*

Francesco Maluta − *Department of Industrial Chemistry "Toso Montanari" and Center for Chemical Catalysis − C3, Alma Mater Studiorum, Università di Bologna, Bologna 40136, Italy*

Andrea Canciani − *Department of Industrial Chemistry "Toso Montanari" and Center for Chemical Catalysis − C3, Alma Mater Studiorum, Università di Bologna, Bologna 40136, Italy*

Francesca Ospitali − *Department of Industrial Chemistry "Toso Montanari", Università di Bologna, Bologna 40136, Italy*

Phuoc H. Ho − *Department of Industrial Chemistry "Toso Montanari", Università di Bologna, Bologna 40136, Italy*

Alessandro Paglianti − *Department of Industrial Chemistry "Toso Montanari", Università di Bologna, Bologna 40136, Italy;* orcid.org/0000-0003-3295-9227

Axel Knop-Gericke − *Fritz-Haber-Institut der Max-Planck-Gesellschaft, Berlin 14195, Germany; Max Planck Institute for Chemical Energy Conversion, Mülheim 45470, Germany*

Giuseppe Fornasari − *Department of Industrial Chemistry "Toso Montanari" and Center for Chemical Catalysis − C3, Alma Mater Studiorum, Università di Bologna, Bologna 40136, Italy*

Complete contact information is available at: https://pubs.acs.org/10.1021/acscatal.3c03363

Funding

This work was funded by the "Alma Idea" project from the Alma Mater Studiorum-University of Bologna.

Notes

The authors declare no competing financial interest.

■ ACKNOWLEDGMENTS

The authors thank Dr. Franco Corticelli for the FE-SEM measurements. We thank the Helmholtz-Zentrum Berlin für Materialien und Energie for the allocation of synchrotron radiation beamtime. We thank Sven Kubala for his help in the preparation of the PVD Cu electrodes on SiN_x windows.

■ REFERENCES

(1) Montini, T.; Melchionna, M.; Monai, M.; Fornasiero, P. Fundamentals and Catalytic Applications of CeO_2-Based Materials. *Chem. Rev.* **2016**, *116*, 5987−6041.

(2) Song, X.-Z.; Zhu, W.-Y.; Wang, X.-F.; Tan, Z. Recent Advances of CeO_2-Based Electrocatalysts for Oxygen and Hydrogen Evolution as well as Nitrogen Reduction. *ChemElectroChem.* **2021**, *8*, 996−1020.

(3) Lu, G.; Zheng, H.; Lv, J.; Wang, G.; Huang, X. Review of recent research work on CeO_2-based electrocatalysts in liquid-phase electrolytes. *J. Power Sources* **2020**, *480*, No. 229091.

(4) Wang, J.; Xiao, X.; Liu, Y.; Pan, K.; Pang, H.; Wei, S. The application of CeO_2-based materials in electrocatalysis. *J. Mater. Chem. A* **2019**, *7*, 17675−17702.

(5) Yu, J.; Du, X.; Liu, H.; Qiu, C.; Yu, R.; Li, S.; Ren, J.; Yang, S. Mini Review on Active Sites in Ce-Based Electrocatalysts for Alkaline Water Splitting. *Energy Fuels* **2021**, *35*, 19000−19011.

(6) Zhiani, M.; Kamali, S. Synergistic effect of ceria on the structure and hydrogen evolution activity of nickel nanoparticles grown on reduced graphene oxide. *J. Mater. Chem. A* **2017**, *5*, 8108−8116.

(7) Sun, Z.; Zhang, J.; Xie, J.; Wang, M.; Zheng, X.; Zhang, Z.; Li, X.; Tang, B. A 3D porous Ni-CeO_2 nanosheet array as a highly efficient Electrocatalyst toward alkaline hydrogen evolution. *Dalton Trans.* **2018**, *47*, 12667−12670.

(8) Arabaci, E. D.; Önal, A. M.; Özkar, S. Ceria Supported Nickel(0) Nanoparticles: A Highly Active and Low Cost Electrocatalyst for Hydrogen Evolution Reaction. *J. Electrochem. Soc.* **2020**, *167*, 106513 DOI: 10.1149/1945-7111/ab9d93.

(9) Demir, E.; Akbayrak, S.; Önal, A. M.; Özkar, S. Nanoceria-Supported Ruthenium(0) Nanoparticles: Highly Active and Stable Catalysts for Hydrogen Evolution from Water. *ACS Appl. Mater. Interface* **2018**, *10*, 6299−6308.

(10) Wang, W.; Tao, Y.; Wu, X.; Yang, L. Flower-like CeO_2-supported small-sized Ru nanoparticle hybrids for highly efficient alkaline hydrogen evolution: Roles of interfacial effects. *Appl. Surf. Sci.* **2022**, *581*, No. 152256.

(11) Ding, Y.; Huang, L.; Zhang, J.; Guan, A.; Wang, Q.; Qian, L.; Zhang, L.; Zheng, G. Ru-doped, oxygen-vacancy-containing CeO_2 nanorods toward N_2 electroreduction. *J. Mater. Chem. A* **2020**, *8*, 7229−7234.

(12) Gao, D.; Zhang, Y.; Zhou, Z.; Cai, F.; Zhao, X.; Huang, W.; Li, Y.; Zhu, J.; Liu, P.; Yang, F.; Wang, G.; Bao, X. Enhancing CO_2 electroreduction with the metal-oxide interface. *J. Am. Chem. Soc.* **2017**, *139*, 5652−5655.

(13) Liu, G.; Cui, Z.; Han, M.; Zhang, S.; Zhao, C.; Chen, C.; Wang, G.; Zhang, H. Ambient Electrosynthesis of Ammonia on a Core−Shell-Structured Au@CeO_2 Catalyst: Contribution of Oxygen Vacancies in CeO_2. *Chem. Eur. J.* **2019**, *25*, 5904−5911, DOI: 10.1002/chem.201806377.

(14) Wang, Y.; Chen, Z.; Han, P.; Du, Y.; Gu, Z.; Xu, X.; Zheng, G. Single-Atomic Cu with Multiple Oxygen Vacancies on Ceria for Electrocatalytic CO_2 Reduction to CH_4. *ACS Catal.* **2018**, *8*, 7113−7119.

(15) Jiang, S.; Zhang, R.; Liu, H.; Rao, Y.; Yu, Y.; Chen, S.; Yue, Q.; Zhang, Y.; Kang, Y. Promoting Formation of Oxygen Vacancies in Two-Dimensional Cobalt-Doped Ceria Nanosheets for Efficient Hydrogen Evolution. *J. Am. Chem. Soc.* **2020**, *142*, 6461−6466.

(16) Xie, H.; Wang, H.; Geng, Q.; Xing, Z.; Wang, W.; Chen, J.; Ji, L.; Chang, L.; Wang, Z.; Mao, J. Oxygen vacancies of Cr-doped CeO_2 nanorods that efficiently enhance the performance of electrocatalytic N_2 fixation to NH_3 under ambient conditions. *Inorg. Chem.* **2019**, *58*, 5423−5427.

(17) Wu, D.; Wen, M.; Gu, C.; Wu, Q. 2D NiFe/CeO_2 Basic-Site-Enhanced Catalyst via in-Situ Topotactic Reduction for Selectively Catalyzing the H_2 Generation from $N_2H_4{\cdot}H_2O$. *ACS Appl. Mater. Interfaces* **2017**, *9*, 16103−16108.

(18) Wei, X.; Wen, X.; Liu, Y.; Chen, C.; Xie, C.; Wang, D.; Qiu, M.; He, N.; Zhou, P.; Chen, W.; Cheng, J.; Lin, H.; Jia, J.; Fu, X.-Z.; Wang, S. Oxygen Vacancy-Mediated Selective C−N Coupling toward Electrocatalytic Urea Synthesis. *J. Am. Chem. Soc.* **2022**, *144*, 11530−11535.

(19) Varandili, S. B.; Huang, J.; Oveisi, E.; De Gregorio, G. L.; Mensi, M.; Strach, M.; Vavra, J.; Gadiyar, C.; Bhowmik, A.; Buonsanti, R. Synthesis of Cu/CeO_{2-x} Nanocrystalline Heterodimers with Interfacial Active Sites To Promote CO_2 Electroreduction. *ACS Catal.* **2019**, *9*, 5035−5046.

(20) Luo, M.; Wang, Z.; Li, Y. C.; Li, J.; Li, F.; Lum, Y.; Nam, D.-H.; Chen, B.; Wicks, J.; Xu, A.; Zhuang, T.; Leow, W. R.; Wang, X.; Dinh, C.-T.; Wang, Y.; Wang, Y.; Sinton, D.; Sargent, E. H. Hydroxide promotes carbon dioxide electroreduction to ethanol on copper via tuning of adsorbed hydrogen. *Nat. Commun.* **2019**, *10*, 5814.

(21) Valenti, G.; Melchionna, M.; Montini, T.; Boni, A.; Nasi, L.; Fonda, E.; Criado, A.; Zitolo, A.; Voci, S.; Bertoni, G.; Bonchio, M.; Fornasiero, P.; Paolucci, F.; Prato, M. Water-Mediated Electro-Hydrogenation of CO_2 at Near-Equilibrium Potential by Carbon Nanotubes/Cerium Dioxide Nanohybrids. *ACS Appl. Energy Mater.* **2020**, *3*, 8509−8518.

(22) Zhou, X.; Shan, J.; Chen, L.; Xia, B. Y.; Ling, T.; Duan, J.; Jiao, Y.; Zheng, Y.; Qiao, S.-Z. Stabilizing Cu^{2+} Ions by Solid Solutions to Promote CO_2 Electroreduction to Methane. *J. Am. Chem. Soc.* **2022**, *144*, 2079−2084.

(23) Akhade, S. A.; Singh, N.; Gutiérrez, O. Y.; Lopez-Ruiz, J.; Wang, H.; Holladay, J. D.; Liu, Y.; Karkamkar, A.; Weber, R. S.; Padmaperuma,

A. B.; Lee, M.-S.; Whyatt, G. A.; Elliott, M.; Holladay, J. E.; Male, J. L.; Lercher, J. A.; Rousseau, R.; Glezakou, V.-A. Electrocatalytic Hydrogenation of Biomass-Derived Organics: A Review. *Chem. Rev.* **2020**, *120*, 11370−11419.
(24) Bender, M. T.; Yuan, X.; Goetz, M. K.; Choi, K.-S. Electrochemical Hydrogenation, Hydrogenolysis, and Dehydrogenation for Reductive and Oxidative Biomass Upgrading Using 5-Hydroxymethylfurfural as a Model System. *ACS Catal.* **2022**, *12*, 12349−12368.
(25) Pang, X.; Zhao, H.; Huang, Y.; Liu, Y.; Bai, H.; Fan, W.; Shi, W. In Situ Electrochemical Reconstitution of CF−CuO/CeO_2 for Efficient Active Species Generation. *Inorg. Chem.* **2022**, *61*, 8940−8954.
(26) Roylance, J. J.; Kim, T. W.; Choi, K.-S. Efficient and Selective Electrochemical and Photoelectrochemical Reduction of 5-Hydroxymethylfurfural to 2,5-Bis(hydroxymethyl)furan using Water as the Hydrogen Source. *ACS Catal.* **2016**, *6*, 1840−1847.
(27) Lee, D. K.; Kubota, S. R.; Janes, A. N.; Bender, M. T.; Woo, J.; Schmidt, J. R.; Choi, K.-S. The Impact of 5-Hydroxymethylfurfural (HMF)-Metal Interactions on the Electrochemical Reduction Pathways of HMF on Various Metal Electrodes. *ChemSusChem* **2021**, *14*, 4563−4572.
(28) Zhang, L.; Zhang, F.; Michel, F. C., Jr; Co, A. C. Efficient Electrochemical Hydrogenation of 5-Hydroxymethylfurfural to 2,5-Bis(hydroxymethyl)furan on Ag-Displaced Nanotextured Cu Catalysts. *ChemElectroChem* **2019**, *6*, 4739−4749.
(29) Liu, H.; Lee, T.-H.; Chen, Y.; Cochran, E. W.; Li, W. Paired and Tandem Electrochemical Conversion of 5-(Hydroxymethyl)furfural Using Membrane-Electrode Assembly-Based Electrolytic Systems. *ChemElectroChem* **2021**, *8*, 2817−2824.
(30) Chadderdon, X. H.; Chadderdon, D. J.; Pfennig, T.; Shanks, B. H.; Li, W. Paired electrocatalytic hydrogenation and oxidation of 5-(hydroxymethyl)furfural for efficient production of biomass-derived monomers. *Green Chem.* **2019**, *21*, 6210−6219.
(31) Sanghez de Luna, G.; Ho, P. H.; Sacco, A.; Hernaández, S.; Velasco-Vélez, J.-J.; Ospitali, F.; Paglianti, A.; Albonetti, S.; Fornasari, G.; Benito, P. AgCu Bimetallic Electrocatalysts for the Reduction of Biomass-Derived Compounds. *ACS Appl. Mater. Interfaces* **2021**, *13*, 23675−23688.
(32) Ji, K.; Xu, M.; Xu, S.-M.; Wang, Y.; Ge, R.; Hu, X.; Sun, X.; Duan, H. Electrocatalytic Hydrogenation of 5-Hydroxymethylfurfural Promoted by a Ru1Cu Single-Atom Alloy Catalyst. *Angew. Chem., Int. Ed.* **2022**, *61*, No. e202209849.
(33) Li, L.; Chen, F.; Lu, J. Q.; Luo, M. F. Study of defect sites in $Ce_{1-x}M_xO_{2-\delta}$ (x = 0.2) solid solutions using Raman spectroscopy. *J. Phys. Chem. A* **2011**, *115*, 7972−7977.
(34) Taniguchi, T.; Watanabe, T.; Sugiyama, N.; Subramani, A. K.; Wagata, H.; Matsushita, N.; Yoshimura, M. Identifying Defects in Ceria-Based Nanocrystals by UV Resonance Raman Spectroscopy. *J. Phys. Chem. C* **2009**, *113*, 19789−19793.
(35) Sanghez de Luna, G.; Ho, P. H.; Lolli, A.; Ospitali, F.; Albonetti, S.; Fornasari, G.; Benito, P. Ag Electrodeposited on Cu Open-Cell Foams for the Selective Electroreduction of 5-Hydroxymethylfurfural. *ChemElectroChem* **2020**, *7*, 1238−1247.
(36) Yuan, X.; Lee, K.; Bender, M. T.; Schmidt, J. R.; Choi, K.-S. Mechanistic Differences between Electrochemical Hydrogenation and Hydrogenolysis of 5-Hydroxymethylfurfural and Their pH Dependence. *ChemSusChem* **2022**, *15*, No. e202200952.
(37) Zhang, D.-F.; Zhang, H.; Guo, L.; Zheng, K.; Han, X.-D.; Zhang, Z. Delicate control of crystallographic facet-oriented Cu_2O nanocrystals and the correlated adsorption ability. *J. Mater. Chem.* **2009**, *19*, 5220−5225.
(38) Ho, P. H.; Ambrosetti, M.; Groppi, G.; Tronconi, E.; Fornasari, G.; Vaccari, A.; Benito, P. Electrodeposition of CeO_2 and Pd-CeO_2 on small pore size metallic foams: Selection of deposition parameters. *Catal. Today* **2019**, *334*, 37−47.
(39) Weng, Z.; Liu, W.; Yin, L.-C.; Fang, R.; Li, M.; Altman, E. I.; Fan, Q.; Li, F.; Cheng, H.-M.; Wang, H. Metal/Oxide Interface Nanostructures Generated by Surface Segregation for Electrocatalysis. *Nano Lett.* **2015**, *15*, 7704−7710.
(40) Liu, M.; Ji, Z.; Shen, X.; Zhou, H.; Zhu, J.; Xie, X.; Song, C.; Miao, X.; Kong, L.; Zhu, G. An Electrocatalyst for a Hydrogen Evolution Reaction in an Alkaline Medium: Three-Dimensional Graphene Supported CeO_2 Hollow Microspheres. *Eur. J. Inorg. Chem.* **2018**, *2018* (35), 3952−3959.
(41) Melchionna, M.; Bevilacqua, M.; Fornasiero, P. The electrifying effects of carbon-CeO_2 interfaces in (electro)catalysis. *Mater. Today Adv.* **2020**, *6*, No. 100050.
(42) Velasco-Vélez, J.-J.; Skorupska, K.; Frei, E.; Huang, Y.-C.; Dong, C.-L.; Su, B.-J.; Hsu, C.-J.; Chou, H.-Y.; Chen, J.-M.; Strasser, P.; Schlögl, R.; Knop-Gericke, A.; Chuang, C.-H. The Electro-Deposition/Dissolution of $CuSO_4$ Aqueous Electrolyte Investigated by *In Situ* Soft X-ray Absorption Spectroscopy. *J. Phys. Chem. B* **2018**, *122*, 780−787.
(43) Garvie, L. A. J.; Buseck, P. R. Determination of Ce^{4+}/Ce^{3+} in electron-beam-damaged CeO_2 by electron energy-loss spectroscopy. *J. Phys. Chem. Solids* **1999**, *60*, 1943−1947.

https://doi.org/10.1021/acscatal.3c03363
ACS Catal. 2023, 13, 12737−12745